Chemical Physics 543 (2021) 111071

Contents lists available at ScienceDirect

Chemical Physics

journal homepage: www.elsevier.com/locate/chemphys

# Initial degradation mechanism of salicylic acid via electrochemical process

Ngoc Lan Mai [a], Noëmi Ambauen [b], Cynthia Hallé [b], Thomas Meyn [b], Thuat T. Trinh [b,*]

[a] Faculty of Applied Sciences, Ton Duc Thang University, Ho Chi Minh City, Viet Nam
[b] Department of Civil and Environmental Engineering, NTNU, Norway

ARTICLE INFO

*Keywords:*
Electrochemical advanced oxidation process
DFT
Salicylic acid
Hydroxylation
Degradation

ABSTRACT

Salicylic acid is a common chemical used in the pharmaceutical industry. Much attention has been paid in recent years to the elimination of this contaminant from the water by electrochemical oxidation. However, there is still a debate about its intermediate products during the degradation process. The goal of this work was to provide further insight into the degradation of salicylic acid by the Density Functional Theory calculations. The detailed mechanism shall be investigated along with the most suitable intermediate products during the process. The results provide an explanation for the experimental observation of 2,3-dihydroxybenzoic acid and 2,5-dihydroxybenzoic acid over other derivatives.

## 1. Introduction

Today thousands of tons of drugs are consumed daily and the residual of this drug still exists in low concentration in surface, ground and even drinking waters. This could cause some problems. In order to prevent adverse health effects on humans and animals, it is increasingly important to eliminate the excess of pharmaceutical drugs in wastewater [1–4]. Salicylic acid (SA) is one of the common drug component in many pharmaceutical and cosmetic products. This compound is the interested subject to remove from wastewater by different oxidation process such as ozonation and electrochemical advanced oxidation process (EAOP) [5–7]. The principal of these technologies is using hydroxyl radical as oxidant to degrade the pollutant into smaller species [8]. Various experimental studies were devoted to investigating the salicylic acid degradation by oxidation processes. Albarranm et al. [9] reported that several species such as 2,3-dihydroxybenzoic acid (23dHBA), 2,4-dihydroxybenzoic acid (24dHBA), 2,5-dihydroxybenzoic acid (25dHBA), 2,6-dihydroxybenzoic acid (26dHBA) and pyrocatechol (CAT) were formed in the radiolytic of SA. A more detail on the transformation of SA via ozonation process was recently investigated by Hu et al. [10]. The author claimed that the main hydroxylation products of SA were 23dHBA, 25dHBA and CAT. Electrochemical advanced oxidation process (EAOP) is one the most promising technologies for wastewater treatment, especially for the sample holding low contents of toxic and organic compounds [11]. One inspiring work of Guine et al. [8] on the use of electrochemical process to degrade the SA was detailed in 2008. By using HPLC/UV and GC/MS techniques, the authors stated that the main intermediate products were 23dHBA, 25dHBA and 26dHBA. Further oxidation could lead to smaller species such as maleic acid, oxalic acid, etc. It is interesting to note that to degrade SA completely into $CO_2$ and water might require 28 electrons. Another investigation by Panchompoo et al. [12] found that the products of the monohydroxylation of SA by Fenton reagent were 23dHBA and 25dHBA species. More recently, Ambauen et al. [5] investigated the effect of $Cl^-$ on the oxidation kinetic of SA with two different anode material such as boron doped diamond (BDD) and Platinum. The intermediate product for the transformation product of SA was reported as 23dHBA, 25dHBA. The formation of 24dHBA, 26dHBA and CAT was not observed even under different reaction conditions [5]. Interestingly, these studies have shown different products on the hydroxylation of salicylic acid, possibly due to different experiments conditions, different reaction mechanisms under different studies. There is limited on the fundamental understanding of this process at atomic level. This has motivated us to this theoretical work to elucidate the initial stage of the degradation of SA, which is the hydroxylation reaction. We will employ quantum chemical calculations to investigate the reaction mechanism as well as reaction free energies and activation barriers. The most favorable intermediate products will be calculated and compared with experimental observations.

## 2. Models and methods

There are commonly two possible pathways for trapping of hydroxyl group by an organic species namely the inverted spin trapping and

* Corresponding author.
*E-mail address:* thuat.trinh@ntnu.no (T.T. Trinh).

https://doi.org/10.1016/j.chemphys.2020.111071
Received 30 July 2020; Received in revised form 11 November 2020; Accepted 4 December 2020
Available online 10 December 2020

Forrester-Hepburn mechanism [3,13,14]. The first one involves a direct electron transfer oxidation reaction of interested molecule (R) as in reaction (1):

$$R \xrightarrow{[-e^-]} R^{\cdot+} \xrightarrow{[+HO^-]} R\text{–}OH \quad (1)$$

In the other hands, the Forrester-Hepburn mechanism is the reverse of this process, which involves nucleophilic attack of molecule (R) by hydroxyl anion followed by direct electron transfer oxidation as described in reaction (2):

$$R \xrightarrow{[+HO^-]} R\text{–}OH^- \xrightarrow{[-e^-]} R\text{–}OH \quad (2)$$

These two mechanisms of hydroxylation reaction were successfully applied for different organic compound by Jing et al. [3]. The authors claimed that the mechanism is different for different chemicals. In the next section, we will show that the hydroxylation mechanism will follow the direct transfer oxidation reaction as defined in Eqs. (1) for our interested compound SA.

We investigated the hydroxylation of SA by using Density Functional Theory calculations. The DFT approach was shown to be consistent with experimental data for several organic compounds [3,15]. All simulations were performed using Gaussian 09 package [16]. We employed B3LYP [17] functional and def2-TZVPP basis set [18] for geometry optimization and transition state (TS) search. Berny algorithm implemented in Gaussian software were used to find the TS. Frequency calculation were done to check the local minimum of the optimized geometry and the transition state. Every transition state search was verified by one and only one imaginary mode in the frequency calculation. The vibration motion was also checked to confirm that the TS was our desirable reaction. From the TS structure, we calculated reaction path by integrating the intrinsic reaction coordinate (IRC) to find the reactant and product geometries. The effect of water was modeled by an implicit solvation using SMD model [19] in both optimization and frequency calculations.

The standard reduction potential of direct electron transfer reaction was calculated as

$$E^0 = -\left(\frac{\Delta_r G^0}{nF}\right) - E^0_{abs}(SHE) \quad (3)$$

Where $\Delta_r G^0$ is the free energy of the reduction reaction, n is the number of electrons transferred, F is the Faraday constant, and $E^0_{abs}(SHE)$ is a reference value for the absolute standard reduction potential of the Standard Hydrogen Electrode. We took the value of $E^0_{abs}(SHE) = 4.28\ eV$ as in the literature [20].

Marcus theory [21] was used to calculate the activation energy $E_a$ vs electrode potential profile for direct electron transfer oxidation reaction according to Eq. (4)

$$E_a = \frac{\lambda_f}{4}\left(1 - \frac{F(E - E^0)}{\lambda_f}\right) \quad (4)$$

$$\lambda_f = E^{charge=R}_{geom=R} - E^{charge=R}_{geom=P} \quad (5)$$

Where E is the electrode potential, $\lambda_f$ is the total reorganization energy for the oxidation reaction. Following the method described in ref [3,22], the values for $\lambda_f$ were calculated by subtracting energy of the reactant from that of a compound with an identical geometry of the product, but with the same charge of reactant state (Eqs. (5)). Thus, this $\lambda_f$ value was mostly the internal reorganization energy. The effect of the solvent on $\lambda_f$ was not considered as previous research showed negligible effects in polar solvents like water [3,22,23]. A similar set up was successful applied to find the standard reduction potential of various organics compounds [3]. To benchmark our setup, we have tried to calculate the standard reduction potential of coumarin (COU). Our method yield $E^0_{COU} = 2.01$ V/SHE, which is in excellent agreement with the value of 2.04 V/SHE by Jing et al. [3].

Fig. 1 presents six different pathways of the electrochemical oxidation of SA. These routes differentiate by the position of the attack of hydroxyl group to the SA. The reaction condition could be different in the later step for dehydrogenation or decarboxylation to form various products. When the tackle occurs on the C3, C4, C5 and C6 positions, there are four products can be formed namely 23dHBA, 24dHBA, 25dHBA and 26dHBA, respectively. Reaction at position C1 may generate pyrocatechol (CAT) after a decarboxylation step. All of these species were experimentally observed in different studies [5,8,12]. Whether the OH group can attract to position C2 is yet unknown. This could lead to an intermediate with the chemical structure as shown in Fig 1. We can predict that there is a possibility of C–C bond dissociation step and a decarboxylation step for that structure. The resulting product can be $CO_2$ molecule and a linear carboxylic acid. However, to study the complete degradation process of SA might be extremely complex and therefore was not the prime focus of this work. We only limited ourselves on the first step of hydroxylation, which is the rate-limiting step of the whole process.

## 3. Results and discussions

### 3.1. Standard reduction potential

We identified two possible configurations during the geometry optimization of SA. There is a less stable one which has no internal hydrogen bonding between the hydroxyl and carboxylic groups. The more stable configuration has that kind of internal hydrogen bonding. Thus, this more favourable geometry of SA was used in our calculation to investigate the reactivity.

Standard reduction potential ($E^0$) is an important property for chemicals in electrochemical process. The chemical with lower $E^0$ can be oxidized first at the anode, the one with higher value will follow later. We calculated the reduction potential of our interesting compounds via Eqs. (3) and presented in Table 1. The values of $E^0$ are in the range of 1.29 V/SHE to 1.81 V/SHE. The largest value is for $E^0_{SA}$. Other structures

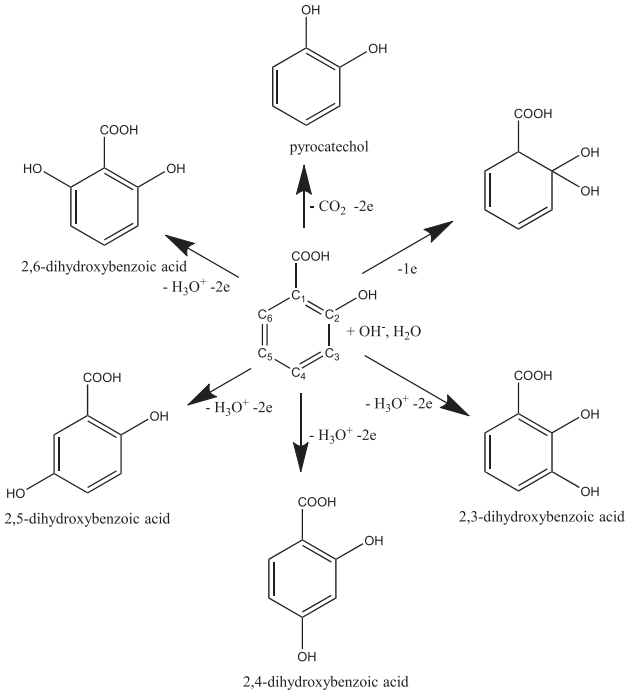


**Fig. 1.** Reaction scheme of hydroxylation reaction of salicyclic acid to form various products in electrochemical process. Most of the product were observed experimentally in the literature. See the text for more details.

**Table 1**
Calculated standard reduction potential, reorganization energy, HOMO, and LUMO energies for different chemical species.

| Structure | $E^0$ (V/SHE) | $\lambda_f$ (kJ/mol) | HOMO (eV) | LUMO (eV) |
|---|---|---|---|---|
| SA | 1.81 | 19 | −6.655 | −1.843 |
| CAT | 1.41 | 29 | −6.241 | −0.338 |
| 23dHBA | 1.44 | 26 | −6.224 | −1.715 |
| 24dHBA | 1.75 | 18 | −6.525 | −1.493 |
| 25dHBA | 1.29 | 21 | −6.045 | −1.776 |
| 26dHBA | 1.50 | 19 | −6.266 | −1.687 |

have a lower value of $E^0$. The reorganization energy $\lambda_f$ together with the energy of HOMO and LUMO were also presented in Table 1. It is interesting to observe that the value of $\lambda_f$ are very similar for most of the structures (19–21 kJ/mol) except for the CAT (29 kJ/mol) and 23dHBA (26 kJ/mol) species. It costs SA around 19 kJ/mol to reorganize the structure in the electrochemical reaction. This value is almost double the energy required for coumarin compound (11 kJ/mol)[3]. However, the $E^0_{SA}$ is smaller than that for the calculated value of coumarin.

This is known that the energy level of HOMO is proportional to the standard reduction potential in many compounds [24]. However, there was a caution that to use this value directly as the calculated potential could get an error up to several voltage [25]. In this work, it is interesting to see the linear relationship between HOMO energy level and the calculated $E^0$ ($R^2 = 0.98$) as depicted in Fig. 2. The electron density plot of HOMO shows that the contribution mostly from oxygen and carbon from the C=C bond (see Fig. 3). There is a minor contribution from the carboxyl group to the HOMO.

Fig. 4 presents the activation energy profiles of the chemicals at different electrode potential. The profile was calculated based on Eqs. (4). For comparison, the profile of ·OH radical formation provided earlier [3,15] was added to the plot. Clearly, ·OH radical formation occurs at higher potential (around 2.3 V/SHE). As a result, SA and other chemicals prefer to reduce and then react with the hydroxyl group $HO^-$. That reaction would be more favorable than the formation of ·OH radical at lower electrode potential. Thus, we will examine that the hydroxylation process of SA with ECE mechanism. The ECE reaction proposed that the oxidation of SA will follow the process of electron transfer reaction, chemical reaction and electron transfer reaction. The ECE was successfully used to explain the hydroxylation of coumarin and similar compounds [3].

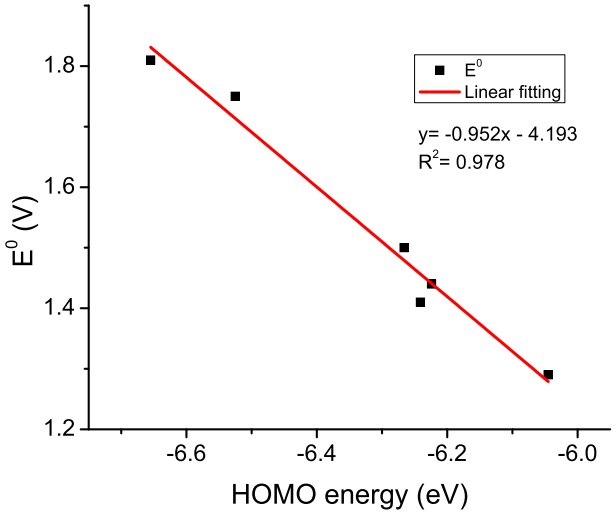


**Fig. 2.** Linear relationship between HOMO energy and calculated standard reduction potential.

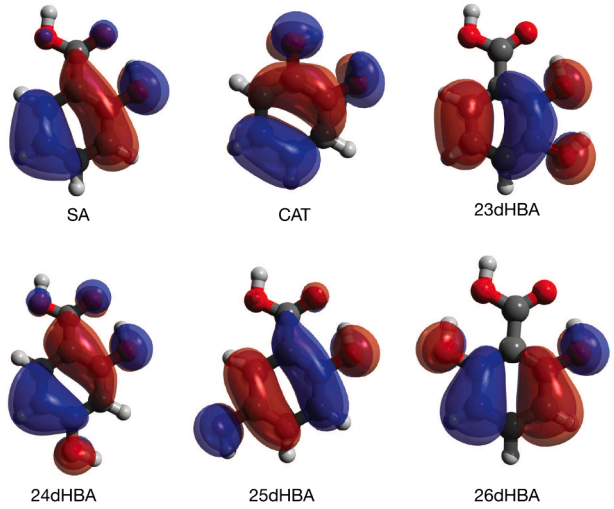


**Fig. 3.** Highest Occupied Molecular Orbital HOMO of various compounds show different contribution of atom to the electron density. The orbital wave functions are positive in the red regions and negative in the blue. The color black, red, white represent for atoms C, O, H, respectively.

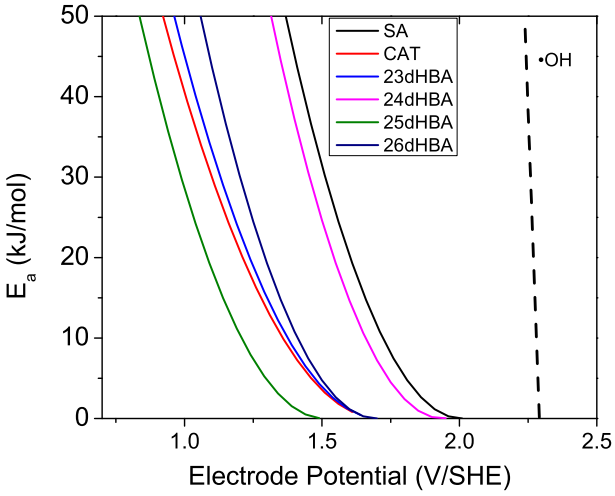


**Fig. 4.** Calculated activation energy Ea vs electrode potential profiles. Profile for ·OH taken from ref [3] for comparison.

### 3.2. Reaction mechanism

The previous section showed that $SA^{\cdot+}$ radical formation is more favorable than ·OH radical. Thus, the attraction of $HO^-$ to the $SA^{\cdot+}$ will be considered as described in the reaction (6).

$$SA \xrightarrow{-e^-} SA^{\cdot+} \xrightarrow{+HO^-} CR \xrightarrow{TS} CP \xrightarrow{-e^- -H_3O^+} P \quad (6)$$

After the formation of $SA^{\cdot+}$ radical, the $HO^-$ will make a pair with $SA^{\cdot+}$ and form a complex reactant (CR). Comparing with the reactant energy, this interaction helps to stabilize the CR structure around 50 kJ/mol to 60 kJ/mol depending on the position C1–C6. The main contribution to the interaction energy is a strong electrostatic interaction between negatively charge of $HO^-$ and positive charge of $SA^{\cdot+}$ radical. In the next step, the formation of C–O bonding between $SA^{\cdot+}$ and $HO^-$ via the transition sate (TS) occurs. It is surprisingly that the activation energy for this step has low activation energy at all positions from C1 to C6. The calculated activation energy $E_a$, which is defined as the difference in free energy between the TS and the CR, is around 15 kJ/mol–18 kJ/mol for position C1, C2, C4, C6. Notably, we obtained a much lower

$E_a$ for the position C3, C5 (only 3 kJ/mol and 5 kJ/mol, respectively). Note that when finding the TS structure, a frequency calculation was always performed to confirm that the TS structure has one and only one imaginary frequency. This vibration mode corresponded to the C–O bond formation. We examined the geometry of the TS and found that the distance C–O in the TS was in the range of 1.86 Å and 2.11 Å (see Fig. 6). This typical C–O distance was also found for the $HO^-$ attraction in various organic compounds [3]. More interestingly, the length of C–O is very similar to that in the CR structures. This implies an early transition state and that in return explains a low activation barrier found in our study.

The free energies of various complex products are reported in Table 2. The data show that most CP are comparably stable within a rage −90 kJ/mol to −100 kJ/mol, except for the C1 position. The CP from C1 position has much less stable structure (−59 kJ/mol) due to bulky geometry constraints. There are two hydroxyl groups and one carboxylic group on C1, so the less stable energy is predictable.

Of the six possible CP structures, further oxidation reaction to release another electron as in the ECE mechanism can occur. This process is triggering with activationless at an electrode potential over 1.81 V/SHE since all the calculated $E^0$ of the CP are in the range of −0.9 V/SHE–1.2 V/SHE. As a result, all complex products are preferable to be oxidized and continue to degrade further. For the next step in degradation process, there are two simple reactions which are $H^+$ transfer and decarboxylation. The product from the $H^+$ transfer reaction of CP of the position C3, C4, C5, C6 are 23dHBA, 24dHBA, 25dHBA, 26dHBA, respectively. Surprisingly, there is a huge different in the stability of the product. It is indeed confirming that the overall reaction to form 23dHBA, 25dHBA are given in reaction (7) and reaction (8), respectively.

$$SA + HO^- \xrightarrow{+H_2O-H_3O^+} 23\ dHBA + 2e, \Delta_r G^0 = -181\ kJ/mol \quad (7)$$

$$SA + HO^- \xrightarrow{+H_2O-H_3O^+} 25\ dHBA + 2e, \Delta_r G^0 = -163\ kJ/mol \quad (8)$$

As shown in Fig. 5, the 23dHBA and 25dHBA are much more energetically stable than 24dHBA and 26dHBA. The energy of 24dHBA and 26dHBA are comparable to its complex product, since there is no gain for further $H^+$ transfer. As a powerful electron donating group, $HO^-$ makes the ortho/para position more electron-rich than other positions. On the other hand, since the single bond -COOH is an electron withdrawing group, it can undergo meta-addition. Both effects on the electron distribution may lead to the enrichment of electrons at position 3,5 more than position 4,6 in the benzene structure. Therefore, in the SA oxidation reaction, the ortho and para positions of the aromatic ring is more stable. This will lead to the formation of 23dHBA and 25dHBA during the oxidation process as observed in experimental work [5].

From the CP on C1 position, the decarboxylation reaction is expected to occur. The result of this step is the CAT structure. Surprisingly, the formation of CAT is very much exothermic. Our DFT results found that CAT is −220 kJ/mol more stable than the initial reactant SA. However, the decarboxylation mechanism can be more complex than the $H^+$ transfer one. Since the former pathway may engage in the C–C bond scission. Therefore, the reaction lead to CAT structure can take longer time to react. There are several experimental report claimed that CAT was formed during the degradation of SA [9,10].

Note that all the products presented here are the intermediate products and will be converted to $CO_2$ and $H_2O$ at the end of the electrochemical oxidation process. From the calculated $E^0$ in Table 1, it is expected that these products will continue to release one more electron with activationless barrier at anodic potential over 1.81 V/SHE. So, the new cycle of ECE mechanism will continue and form various products such as maleic acid, fumaric, malic oxalic acid, glycolic acid, etc... as observed in experimental [8]. However, as shown in several works [5,8,10], the rate limiting step of the whole process is the hydroxylation.

In addition to the ECE mechanism, we also tried out other mechanisms. For example, the CE pathway with the first step is the nucleophilic addition of the hydroxyl group to the SA described in the reaction (2). Unsurprisingly, due to the strong steric effect of the positions C1 and C2, the nucleophilic attack of the hydroxyl groups on the C1, C2 leads to unstable products (the optimization process always results in the stable reactant state of SA and hydroxyl). The combination of $HO^-$ with positions C3, C4, C5 and C6 produced very high activation barriers in the range of 78–252 kJ/mol. These barriers to activation are much higher than the ECE mechanism. This again indicates that the ECE is more advantageous. Therefore, we only reported the most stable pathway involving the ECE mechanism as presented in Fig. 5.

**Table 2**
Relative free energy (kJ/mol) profile along the hydroxylation reaction of Salicyclic acid at different Carbon atom. The name of the product are CAT, 23dHBA, 24dHBA, 25dHBA, 26dHBA for C1, C3, C4, C5 and C6 positions, respectively.

| Position | C1 | C2 | C3 | C4 | C5 | C6 |
|---|---|---|---|---|---|---|
| $SA^{\cdot+}$ | 0 | 0 | 0 | 0 | 0 | 0 |
| CR | −49 | −54 | −53 | −56 | −55 | −62 |
| TS | −34 | −36 | −50 | −39 | −50 | −47 |
| CP | −59 | −92 | −98 | −90 | −86 | −100 |
| P | −220 | / | −181 | −90 | −163 | −86 |

## 4. Conclusions

In conclusion, we have performed DFT simulation to investigate all possibilities of the initial hydroxylation of SA in the electrochemical process. The calculated standard reduction potential profile suggested that SA was first oxidized into its radical form during the process. This key step occurs before the formation of $^{\cdot}OH$ with a lower $E^0$ than that of $^{\cdot}OH$ radical formation. The attack of $HO^-$ anion to 6 possible positions from C1 to C6 of the $SA^{\cdot+}$ radical was all thermodynamically favorable. DFT results reported that the hydroxylation on C3, C5 positions are more kinetically favorable than that on C4, C6 positions. The resulting of this step are six different complex products. However, further reactions are different. Started from the most fundamental reaction, which is $H^+$ transfer, the most stable products are 23dHBA and 25dHBA species.

The calculated results are in excellent agreement with experimental observations that only 23dHBA and 25dHBA were detectable in the oxidation SA with BDD and Platinum electrodes [5,10]. While the 24dHBA, 26dHBA were rarely seen in the experiment. From the DFT calculation, we can conclude that the formation of 2,3 and 2,5 are both thermodynamically and kinetically more encouraging than that of 24dHBA and 26dHBA species.

It is important to note that starting from the complex product at position C1, a further decarboxylation reaction can lead to catechol product with an overall exothermic reaction of −220 kJ/mol. This observation is in line with other experiments' work [10].

The further reaction can happen to completely degrade the SA into smaller species such as organic acid, $CO_2$, and water. Our calculated $E^0$ of Catechol, 23dHBA, 24dHBA, 25dHBA, and 26dHBA species were in the range of 1.29 V/SHE–1.41 V/SHE. These values are lower than the $E^0$ of $^{\cdot}OH$ radical formation. This suggested that further oxidation process by one electron transfer can occurs spontaneously. A new ECE cycle to continue the degradation of these intermediate product are expected. It is note that the full oxidation process of SA to $CO_2$ and $H_2O$ can require up to 28 electrons to complete [8]. Thus, to provide a more detailed picture of the full process, further investigation is required.

## CRediT authorship contribution statement

**Ngoc Lan Mai:** Writing - original draft, Methodology, Software, Investigation. **Noëmi Ambauen:** Investigation, Validation. **Cynthia Hallé:** Investigation, Validation, Funding acquisition. **Thomas Meyn:**

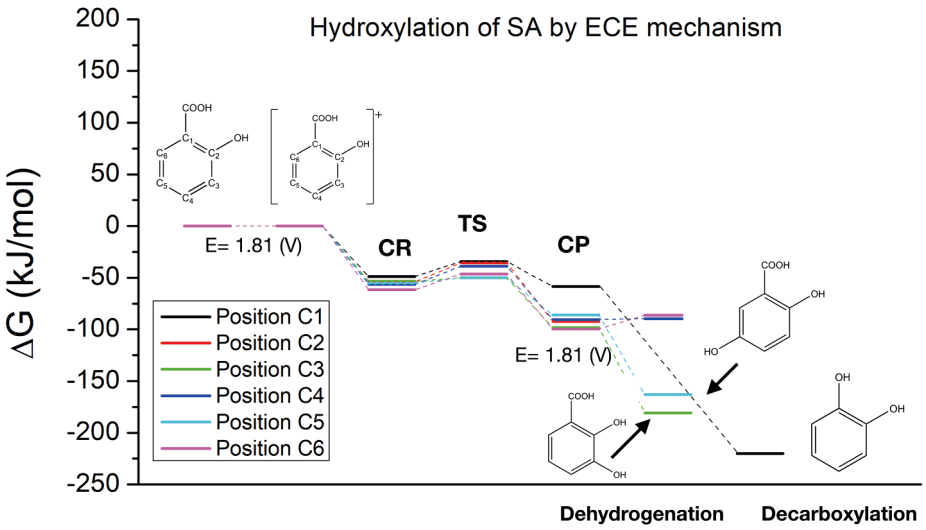


**Fig. 5.** Free energy profile of the hydroxylation process of Salicyclic acid. CR, TS and CP stand for Complex Reactant, Transition State and Complex Product, respectively. The profile indicates the 23dHBA and 25dHBA are the most stable products after $H^+$ transfer, while Catechol is stable after decarboxylation.

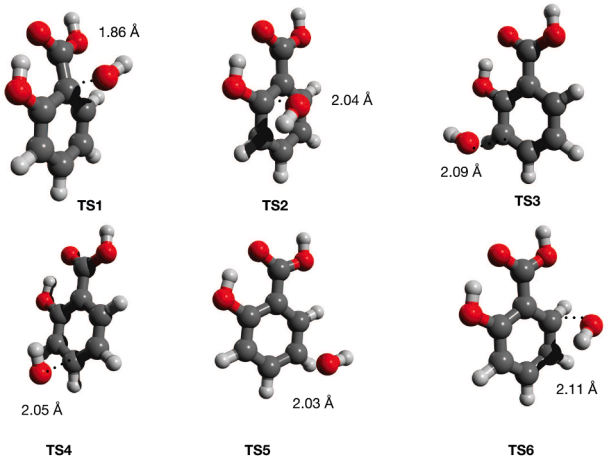


**Fig. 6.** Geometry of the Transition state of the chemical reaction step by ECE mechanism. The color black, red, white represent for atoms C, O, H, respectively. The distance between C and O atoms corresponding to the bond creation between SA and hydroxyl group are shown.

Investigation, Validation, Funding acquisition. **Thuat T. Trinh:** Conceptualization, Validation, Supervision, Resources, Writing - review & editing.

## Declaration of Competing Interest

The authors declare that they have no known competing financial interests or personal relationships that could have appeared to influence the work reported in this paper.

## Acknowledgement

The authors would like to thank the Norwegian University of Science and Technology (NTNU) and Søndre Helgeland Miljøverk IKS (SHMIL, Norway) for financial support. The computational resource was partially provided by Ton Duc Thang university and the Norwegian Metacentre for Computational Science (NOTUR) project number nn4554k.

## References

[1] D. Lapworth, N. Baran, M. Stuart, R. Ward, Emerging organic contaminants in groundwater: A review of sources, fate and occurrence, Environ. Pollut. 163 (2012) 287–303, https://doi.org/10.1016/j.envpol.2011.12.034.
[2] E. Carmona, V. Andreu, Y. PicÓ, Occurrence of acidic pharmaceuticals and personal care products in turia river basin: From waste to drinking water, Sci. Total Environ. 484 (2014) 53–63, https://doi.org/10.1016/j.scitotenv.2014.02.085.
[3] Y. Jing, B.P. Chaplin, Mechanistic study of the validity of using hydroxyl radical probes to characterize electrochemical advanced oxidation processes, Environ. Sci. Technol. 51 (4) (2017) 2355–2365, https://doi.org/10.1021/acs.est.6b05513.
[4] N. Ambauen, J. Muff, F. Tscheikner-Gratl, T.T. Trinh, C. Hallé, T. Meyn, Application of electrochemical oxidation in cold climate regions–effect of temperature, ph and anode material on the degradation of bisphenol a and the formation of disinfection by-products, J. Environ. Chem. Eng. (2020), 104183.
[5] N. Ambauen, J. Muff, N.L. Mai, C. Hallé, T.T. Trinh, T. Meyn, Insights into the kinetics of intermediate formation during electrochemical oxidation of the organic model pollutant salicylic acid in chloride electrolyte, Water 11 (7) (2019) 1322, https://doi.org/10.3390/w11071322.
[6] C. Magro, E.P. Mateus, J.M. Paz-Garcia, A.B. Ribeiro, Emerging organic contaminants in wastewater: Understanding electrochemical reactors for triclosan and its by-products degradation, Chemosphere 247 (2020) 125758. doi:10.1016/j.chemosphere.2019.125758.
[7] J. Karpińska, U. Kotowska, Removal of organic pollution in the water environment, Water 11 (2019) 2017, https://doi.org/10.3390/w11102017.
[8] E. Guinea, C. Arias, P.L. Cabot, J.A. Garrido, R.M. Rodríguez, F. Centellas, E. Brillas, Mineralization of salicylic acid in acidic aqueous medium by electrochemical advanced oxidation processes using platinum and boron-doped diamond as anode and cathodically generated hydrogen peroxide, Water Res. 42 (1–2) (2008) 499–511, https://doi.org/10.1016/j.watres.2007.07.046.
[9] G. Albarran, R. Schuler, Concerted effects in the reaction of OH radicals with aromatics: Radiolytic oxidation of salicylic acid, Radiat. Phys. Chem. 67 (3–4) (2003) 279–285, https://doi.org/10.1016/s0969-806x(03)00052-5.
[10] R. Hu, L. Zhang, J. Hu, Study on the kinetics and transformation products of salicylic acid in water via ozonation, Chemosphere 153 (2016) 394–404, https://doi.org/10.1016/j.chemosphere.2016.03.074.
[11] M.A. Tarr, Chemical Degradation Methods for Wastes and Pollutants: Environmental and Industrial Applications, CRC Press, 2003.
[12] J. Panchompoo, L. Aldous, M. Kabeshov, B.S. Pilgrim, T.J. Donohoe, R.G. Compton, A green approach to fenton chemistry: Mono-hydroxylation of salicylic acid in aqueous medium by the electrogeneration of fenton's reagent, New J. Chem. 36 (5) (2012) 1265, https://doi.org/10.1039/c2nj21007j.
[13] C.D. Jaeger, A.J. Bard, Spin trapping and electron spin resonance detection of radical intermediates in the photodecomposition of water at titanium dioxide particulate systems, J. Phys. Chem. 83 (24) (1979) 3146–3152, https://doi.org/10.1021/j100487a017.
[14] A. Forrester, S. Hepburn, Spin traps. a cautionary note, J. Chem. Soc., C (1971) 701, https://doi.org/10.1039/j39710000701.
[15] B.P. Chaplin, D.K. Hubler, J. Farrell, Understanding anodic wear at boron doped diamond film electrodes, Electrochim. Acta 89 (2013) 122–131, https://doi.org/10.1016/j.electacta.2012.10.166.
[16] M. Frisch, G.W. Trucks, H.B. Schlegel, G.E. Scuseria, M.A. Robb, J.R. Cheeseman, G. Scalmani, V. Barone, B. Mennucci, G. e. Petersson, et al., Gaussian 09 revision d. 01 (2014).

[17] C. Lee, W. Yang, R.G. Parr, Development of the colle-salvetti correlation-energy formula into a functional of the electron density, Phys. Rev. B 37 (2) (1988) 785–789, https://doi.org/10.1103/physrevb.37.785.
[18] F. Weigend, F. Furche, R. Ahlrichs, Gaussian basis sets of quadruple zeta valence quality for atoms h–Kr, J. Chem. Phys. 119 (24) (2003) 12753–12762, https://doi.org/10.1063/1.1627293.
[19] A.V. Marenich, C.J. Cramer, D.G. Truhlar, Universal solvation model based on solute electron density and on a continuum model of the solvent defined by the bulk dielectric constant and atomic surface tensions, J. Phys. Chem. B 113 (18) (2009) 6378–6396, https://doi.org/10.1021/jp810292n.
[20] C.P. Kelly, C.J. Cramer, D.G. Truhlar, Single-ion solvation free energies and the normal hydrogen electrode potential in methanol, acetonitrile, and dimethyl sulfoxide, J. Phys. Chem. B 111 (2) (2007) 408–422, https://doi.org/10.1021/jp065403l.
[21] A.J. Bard, L.R. Faulkner, J. Leddy, C.G. Zoski, Electrochemical methods: Fundamentals and applications, vol. 2, Wiley New York, 1980.
[22] M.-H. Lin, D.M. Bulman, C.K. Remucal, B.P. Chaplin, Chlorinated byproduct formation during the electrochemical advanced oxidation process at magneli phase ti4o7 electrodes, Environ. Sci. Technol. 54 (19) (2020) 12673–12683.
[23] V. Vaissier, P. Barnes, J. Kirkpatrick, J. Nelson, Influence of polar medium on the reorganization energy of charge transfer between dyes in a dye sensitized film, Phys. Chem. Chem. Phys. 15 (13) (2013) 4804–4814.
[24] S.-S. Sun, L.R. Dalton, Introduction to Organic Electronic and Optoelectronic Materials and Devices, CRC Press (2008), https://doi.org/10.1201/9781420009194.
[25] P. Peljo, H.H. Girault, Electrochemical potential window of battery electrolytes: The HOMO–LUMO misconception, Energy Environ. Sci. 11 (9) (2018) 2306–2309, https://doi.org/10.1039/c8ee01286e.